Studies in X-Ray Production by Proton Bombardment of C, Mg, Al, Nd, Sm, Gd, Tb, Dy, and Ho†

J. M. KHAN, D. L. POTTER, AND R. D. WORLEY
Lawrence Radiation Laboratory, University of California, Livermore, California
(Received 30 April 1965)

Thick-target yields, x-ray production, and ionization cross sections are presented for nine elements bombarded with protons of 15- to 1900-keV energy. The measurements are made by observing the x-ray emission (proportional-counter detection) when protons are stopped in thick samples of the target material. The x rays are produced in K, L, and M shells: C(K), Mg(K), and Al(K) in the intervals 15–110 keV and 500–1900 keV; Nd(L), Sm(L), Gd(L), Tb(L), Dy(L), and Ho(L) in the interval 500–1700 keV; Nd(M), Sm(M), Gd(M), Tb(M), Dy(M), and Ho(M) in the intervals 25–100 keV and 500–1700 keV. Where available, previous results are included to complete the presentation for these elements. A study of carbon-contamination buildup is included as an appendix.

INTRODUCTION

THE present work is part of a series of measurements directed toward the study of the production of soft x rays by proton bombardment.[1,2] The general features of the experimental method and apparatus have previously been discussed.[1] As a result, only aspects of the experiments of special interest will be included here.

The present data complete the study of the elements and shells reported. In the K shell, C, Mg, and Al have been studied over the range from 15 to 1900 keV; in the M shell, Nd, Sm, Gd, Tb, Dy, and Ho have been studied over the same energy interval. L-shell results for the six rare-earth elements are also presented above 500 keV.

One of the purposes of these studies is to ascertain the validity of the currently available theoretical descriptions of this class of inelastic proton scattering. The conventional approach for hard x-ray production processes at high (>0.5 MeV) bombarding energies is the Born approximation.[3] This calculation appears to fail below 500 keV.[4] An alternative calculation employs a classical description of the proton trajectory given by Bang and Hansteen.[5] This latter calculation has been performed only for the K shell at present although Merzbacher is considering L- and M-shell calculations.[6] To compare the two descriptions, the case of aluminum is considered. The authors have made a preliminary evaluation of the Bang and Hansteen calculation up to 300 keV. Below this energy both descriptions produce values for the ionization cross sections that exceed the experimental. Above 300 keV the Born-approximation values fall within the experimental error.

APPARATUS AND METHOD

Some of the experimental apparatus used in the present measurements has been discussed elsewhere.[1,2] There are a number of special features (i.e., x-ray energies, proton energies, and refinement of previous techniques) that pertain to the present operating ranges. The proton sources will be briefly described as well as calibration methods. The detector electronics, counting gases and pressures, and counter-window materials will also be discussed.

The measurements were made in two distinct energy ranges, each requiring separate accelerators. Protons in the 0–100-keV region were supplied by an accelerator which employed a conventional rf electrodeless discharge source and a dc power supply (15 mA at voltages up to 120 kV). The potential drop from probe to ground was measured by a precision, temperature-stabilized, 150-MΩ dropping resistor string. A conventional Van de Graaff generator, capable of supplying currents up to 10 μA, provided protons in the 500–1900-keV range. The voltage was monitored by a generating voltmeter which was calibrated against three (p,γ) resonances in a thick target of LiF. (Two of these are shown in Fig. 1.) A 2-in. crystal of NaI mounted on a photomultiplier tube was employed to detect the gamma radiation. An Eldorado (Model C-110) current integrator, which obtained its input from a special target chamber described in previous publications,[1] was used to collect current in both energy ranges.

A flow-mode proportional counter of conventional design was used to detect the x rays. A typical spectrum for aluminum is shown in Fig. 2. The x-ray counting circuit is shown in Fig. 3. The pulses (100-μsec duration) from the proportional counter are inverted and amplified. The differential pulse-height discriminator selects the pulses which are then counted in a scaler. The base line of the discriminator may be set to reduce background counts originating from the noise in the pre-

† This work was performed under the auspices of the U. S. Atomic Energy Commission.

[1] J. M. Khan and D. L. Potter, Phys. Rev. **133**, A890 (1964).

[2] J. M. Khan, D. L. Potter, and R. D. Worley, Phys. Rev. **134**, A316 (1964); **135**, A511 (1964); **136**, A108 (1964); J. M. Khan, D. L. Potter, R. D. Worley, W. Brandt, and H. P. Smith, Jr., Phys. Rev. Letters **14**, 42 (1965).

[3] E. Merzbacher and H. W. Lewis, *Encyclopedia of Physics*, edited by S. Flügge (Springer-Verlag, Berlin, 1958), Vol. 34, p. 166.

[4] R. C. Jopson, Hans Mark, and C. D. Swift, Phys. Rev. **127**, 1612 (1962).

[5] J. Bang and J. M. Hansteen, Kgl. Danske Videnskab. Selskab, Mat. Fys. Medd. **31**, No. 13 (1959).

[6] E. Merzbacher (private communication).

TABLE I. K-shell ionization cross sections.

Element	Z	E_p (keV)	$N(E_p)$ (x rays/μC)	$\frac{\Lambda^a}{T_w A_c}$	I_μ (x rays/ proton)	$\frac{dI_\mu}{dE_p}$ (x ray/ proton keV)	$S(E)^b$ (keV cm^2/ mg)	$\frac{1}{n}\frac{dI_\mu}{dE}S(E)$	$\frac{1}{n}\frac{\mu^c}{\rho}I_\mu$	σ_x (cm^2)	$\sigma_I{}^d$ (cm^2)
Carbon	6	15	7.8	$\frac{(3364)}{(0.050)_w(0.56)_c}$	1.50(−7)	1.11(−8)	75	5.11(−26)	6.50(−27)	5.76(−26)	8.2(−24)
		20	27	$\frac{(3364)}{(0.050)_w(0.56)_c}$	5.18(−7)	3.85(−8)	100	1.77(−25)	2.25(−26)	2.00(−25)	2.9(−23)
K shell		25	62	$\frac{(3364)}{(0.050)_w(0.56)_c}$	1.19(−6)	8.82(−8)	125	5.07(−25)	5.18(−26)	5.58(−25)	8.0(−23)
		30	180	$\frac{(3364)}{(0.050)_w(0.56)_c}$	3.40(−6)	1.40(−7)	150	1.68(−24)	1.47(−25)	1.83(−24)	2.6(−22)
$h\nu \approx 280$ eV		40	610	$\frac{(3364)}{(0.050)_w(0.56)_c}$	1.17(−5)	6.35(−7)	200	5.82(−24)	5.08(−25)	6.33(−24)	9.1(−22)
		50	1700	$\frac{(3364)}{(0.050)_w(0.56)_c}$	3.28(−5)	1.22(−6)	250	1.40(−23)	1.42(−24)	1.53(−23)	2.2(−21)
$\mu/\rho = 2170$ cm^2/g		60	3700	$\frac{(3364)}{(0.050)_w(0.56)_c}$	7.09(−5)	2.25(−6)	300	3.10(−23)	3.07(−24)	3.40(−23)	4.9(−21)
		70	6600	$\frac{(3364)}{(0.050)_w(0.56)_c}$	1.27(−4)	3.35(−6)	350	5.39(−23)	5.51(−24)	5.94(−23)	8.5(−21)
$\omega_K = 0.007$		80	12 000	$\frac{(3364)}{(0.050)_w(0.56)_c}$	2.32(−4)	5.80(−6)	400	1.07(−22)	1.01(−23)	1.17(−23)	1.7(−20)
		90	18 700	$\frac{(3364)}{(0.050)_w(0.56)_c}$	3.58(−4)	7.31(−6)	450	1.51(−22)	1.56(−23)	1.66(−22)	2.4(−20)
		100	25 600	$\frac{(3364)}{(0.050)_w(0.56)_c}$	4.93(−4)	8.01(−6)	500	1.86(−22)	2.14(−23)	2.07(−22)	3.0(−20)
		110	38 900	$\frac{(3364)}{(0.050)_w(0.56)_c}$	7.46(−4)	9.60(−6)	550	2.42(−22)	3.24(−23)	2.74(−22)	3.9(−20)
		499	131 000	$\frac{46\,090}{(0.050)_w(0.56)_c}$	3.43(−2)	1.1 (−4)	310	6.80(−22)	1.49(−21)	2.17(−21)	3.1(−19)
		595	162 000	$\frac{46\,090}{(0.050)_w(0.56)_c}$	4.27(−2)	0.67(−4)	290	3.86(−22)	1.85(−21)	2.24(−21)	3.2(−19)
		698	181 000	$\frac{46\,090}{(0.050)_w(0.56)_c}$	4.77(−2)	0.40(−4)	260	2.08(−22)	2.07(−21)	2.28(−21)	3.3(−19)
		775	192 000	$\frac{46\,090}{(0.050)_w(0.56)_c}$	5.03(−2)	0.20(−4)	250	1.00(−22)	2.18(−21)	2.28(−21)	3.3(−19)
		910	198 000	$\frac{46\,090}{(0.050)_w(0.56)_c}$	5.19(−2)	0.84(−5)	225	3.79(−23)	2.25(−21)	2.29(−21)	3.3(−19)
		1022	198 000	$\frac{46\,090}{(0.050)_w(0.56)_c}$	5.21(−2)	−0.53(−5)	205	−2.18(−23)	2.26(−21)	2.24(−21)	3.2(−19)
		1096	193 000	$\frac{46\,090}{(0.050)_w(0.56)_c}$	5.07(−2)	−0.46(−5)	192	−1.76(−23)	2.20(−21)	2.18(−21)	3.1(−19)
		1196	192 000	$\frac{46\,090}{(0.050)_w(0.56)_c}$	5.05(−2)	−0.46(−5)	180	−1.66(−23)	2.19(−21)	2.17(−21)	3.1(−19)
		1270	188 000	$\frac{46\,090}{(0.050)_w(0.56)_c}$	4.93(−2)	−0.46(−5)	175	−1.61(−23)	2.12(−21)	2.10(−21)	3.0(−19)
		1360	185 000	$\frac{46\,090}{(0.050)_w(0.56)_c}$	4.87(−2)	−0.46(−5)	168	−1.55(−23)	2.11(−21)	2.09(−21)	3.0(−19)
		1505	179 000	$\frac{46\,090}{(0.050)_w(0.56)_c}$	4.69(−2)	−0.46(−5)	156	−1.44(−23)	2.03(−21)	2.02(−21)	2.9(−19)
		1658	172 000	$\frac{46\,090}{(0.050)_w(0.56)_c}$	4.50(−2)	−0.46(−5)	150	−1.38(−23)	1.95(−21)	1.94(−21)	2.8(−19)
		1908	167 000	$\frac{46\,090}{(0.050)_w(0.56)_c}$	4.37(−2)	−0.46(−5)	145	−1.32(−23)	1.90(−21)	1.89(−21)	2.7(−19)
Magnesium	12	25	0.36	$\frac{3364}{(0.173)_w}$	1.12(−9)	3.22(−10)	330	4.29(−27)	1.99(−29)	4.31(−27)	2.0(−25)
		30	1.43	$\frac{3364}{(0.173)_w}$	4.45(−9)	1.02(−9)	371	1.52(−26)	7.89(−29)	1.53(−26)	7.3(−25)
K shell		40	8.46	$\frac{3364}{(0.173)_w}$	2.64(−8)	4.22(−9)	429	7.29(−26)	4.67(−28)	7.34(−26)	3.5(−24)
		50	32.6	$\frac{3364}{(0.173)_w}$	1.02(−7)	1.20(−8)	464	2.25(−25)	1.81(−27)	2.27(−25)	1.1(−23)
$h\nu \approx 1.3$ keV		60	83.4	$\frac{3364}{(0.173)_w}$	2.60(−7)	2.28(−8)	479	4.40(−25)	4.63(−27)	4.45(−25)	2.1(−23)
		70	183	$\frac{3364}{(0.173)_w}$	5.70(−7)	4.32(−8)	484	8.42(−25)	1.01(−26)	8.52(−25)	4.1(−23)
$\mu/\rho = 441$ cm^2/g		80	371	$\frac{3364}{(0.173)_w}$	1.16(−6)	9.43(−8)	482	1.83(−24)	2.06(−26)	1.85(−24)	8.8(−23)
		90	676	$\frac{3364}{(0.173)_w}$	2.11(−6)	1.24(−7)	475	2.37(−24)	3.75(−26)	2.41(−24)	1.2(−22)
$\omega_K = 0.021$		100	1140	$\frac{3364}{(0.173)_w}$	3.56(−6)	1.84(−7)	458	3.40(−24)	6.35(−26)	3.46(−24)	1.6(−22)
		602	46 200	$\frac{3364}{(0.0040)_w}$	6.19(−3)	3.3(−5)	240	3.16(−22)	1.09(−22)	4.25(−22)	2.0(−20)

TABLE I (*continued*)

Element	Z	E_p (keV)	$N(E_p)$ (x rays/μC)	$\frac{\Delta^a}{T_w A_c}$	I_μ (x rays/ proton)	$\frac{dI_\mu}{dE_p}$ (x ray/ proton-keV)	$S(E)^b$ (keV-cm^2/ mg)	$\frac{1}{n}\frac{dI_\mu}{dE}S(E)$	$\frac{1}{n}\frac{\mu^c}{\rho}I_\mu$	σ_x (cm^2)	$\sigma_I{}^d$ (cm^2)
Magnesium (continued)		686	67 200	$\frac{3364}{(0.0040)_w}$	9.01(−3)	3.3(−5)	220	2.90(−22)	1.59(−22)	4.49(−22)	2.1(−20)
		800	99 800	$\frac{3364}{(0.0040)_w}$	1.34(−2)	3.3(−5)	205	2.70(−22)	2.36(−22)	5.06(−22)	2.4(−20)
		900	136 000	$\frac{3364}{(0.0040)_w}$	1.83(−2)	3.3(−5)	192	2.54(−22)	3.23(−22)	5.77(−22)	2.7(−20)
		1000	169 000	$\frac{3364}{(0.0040)_w}$	2.28(−2)	3.3(−5)	182	2.40(−22)	4.02(−22)	6.42(−22)	3.0(−20)
		1100	213 000	$\frac{3364}{(0.0040)_w}$	2.85(−2)	3.3(−5)	170	2.24(−22)	5.03(−22)	7.27(−22)	3.5(−20)
		1200	238 000	$\frac{3364}{(0.0040)_w}$	3.19(−2)	3.3(−5)	160	2.11(−22)	5.62(−22)	7.73(−22)	3.8(−20)
		1310	290 000	$\frac{3364}{(0.0040)_w}$	3.88(−2)	3.3(−5)	148	1.95(−22)	6.84(−22)	8.79(−22)	4.2(−20)
		1400	322 000	$\frac{3364}{(0.0040)_w}$	4.32(−2)	3.3(−5)	140	1.85(−22)	7.61(−22)	9.46(−22)	4.5(−20)
		1500	363 000	$\frac{3364}{(0.0040)_w}$	4.86(−2)	3.3(−5)	131	1.73(−22)	8.56(−22)	1.03(−21)	4.9(−20)
		1600	380 000	$\frac{3364}{(0.0040)_w}$	5.09(−2)	3.3(−5)	129	1.70(−22)	8.96(−22)	1.07(−21)	5.1(−20)
		1700	411 000	$\frac{3364}{(0.0040)_w}$	5.51(−2)	3.3(−5)	125	1.65(−22)	9.72(−22)	1.14(−21)	5.4(−20)
Aluminum	13	25	0.23	$\frac{3364}{(0.34)_w}$	3.68(−10)	1.06(−10)	300	1.42(−27)	6.53(−30)	1.43(−27)	4.9(−26)
		30	0.85	$\frac{3364}{(0.34)_w}$	1.36(−9)	3.29(−10)	337	4.99(−27)	2.42(−29)	5.01(−27)	1.7(−25)
K shell		40	6.42	$\frac{3364}{(0.34)_w}$	1.03(−8)	1.69(−9)	390	2.96(−26)	1.83(−28)	2.98(−26)	1.0(−24)
		50	24.8	$\frac{3364}{(0.34)_w}$	3.97(−8)	4.81(−9)	422	9.12(−26)	7.05(−28)	9.19(−26)	3.2(−24)
$h\nu \approx 1.5$ keV		60	71.0	$\frac{3364}{(0.34)_w}$	1.14(−7)	1.07(−8)	435	2.09(−25)	2.02(−27)	2.11(−25)	7.3(−24)
		70	161	$\frac{3364}{(0.34)_w}$	2.58(−7)	2.05(−8)	440	4.04(−25)	4.59(−27)	4.09(−25)	1.4(−23)
$\mu/\rho = 396$ cm^2/g		80	330	$\frac{3364}{(0.34)_w}$	5.28(−7)	3.49(−8)	438	6.88(−25)	9.39(−27)	6.97(−25)	2.4(−23)
		90	595	$\frac{3364}{(0.34)_w}$	9.52(−7)	5.38(−8)	432	1.04(−24)	1.69(−26)	1.06(−24)	3.7(−23)
$\omega_K = 0.029$		100	1010	$\frac{3364}{(0.34)_w}$	1.61(−6)	8.08(−8)	416	1.51(−24)	2.86(−26)	1.54(−24)	5.3(−23)
		484	3480	$\frac{3364}{(0.0011)_w}$	1.66(−3)	1.45(−5)	250	1.63(−22)	2.90(−23)	1.92(−22)	6.5(−21)
		598	7310	$\frac{3364}{(0.0011)_w}$	3.49(−3)	2.00(−5)	235	2.10(−22)	6.10(−23)	2.72(−22)	9.3(−21)
		700	12 000	$\frac{3364}{(0.0011)_w}$	5.72(−3)	2.60(−5)	210	2.44(−22)	1.00(−22)	3.44(−22)	1.2(−20)
		800	17 900	$\frac{3364}{(0.0011)_w}$	8.52(−3)	3.00(−5)	200	2.68(−22)	1.49(−22)	4.17(−22)	1.4(−20)
		900	24 500	$\frac{3364}{(0.0011)_w}$	1.17(−2)	3.30(−5)	190	2.82(−22)	2.04(−22)	4.86(−22)	1.7(−20)
		1000	31 600	$\frac{3364}{(0.0011)_w}$	1.51(−2)	3.50(−5)	180	2.82(−22)	2.64(−22)	5.46(−22)	1.9(−20)
		1100	39 200	$\frac{3364}{(0.0011)_w}$	1.87(−2)	3.80(−5)	170	2.90(−22)	3.27(−22)	6.17(−22)	2.1(−20)
		1200	47 700	$\frac{3364}{(0.0011)_w}$	2.28(−2)	3.80(−5)	158	2.68(−22)	3.98(−22)	6.66(−22)	2.3(−20)
		1300	56 900	$\frac{3364}{(0.0011)_w}$	2.71(−2)	3.80(−5)	145	2.46(−22)	4.73(−22)	7.19(−22)	2.5(−20)
		1400	63 800	$\frac{3364}{(0.0011)_w}$	3.04(−2)	3.80(−5)	138	2.35(−22)	5.31(−22)	7.66(−22)	2.6(−20)
		1500	72 700	$\frac{3364}{(0.0011)_w}$	3.47(−2)	3.80(−5)	130	2.22(−22)	6.06(−22)	8.28(−22)	2.8(−20)
		1600	80 200	$\frac{3364}{(0.0011)_w}$	3.82(−2)	3.80(−5)	125	2.13(−22)	6.67(−22)	8.80(−22)	3.0(−20)
		1700	86 500	$\frac{3364}{(0.0011)_w}$	4.12(−2)	3.80(−5)	120	2.04(−22)	7.20(−22)	9.24(−22)	3.2(−20)

[a] Δ (geometrical correction factor) $= 4\pi R^2$/area of counter window; T_w (counter window transmission) $\equiv I/I_0$; A_c (counter absorption) $= 1 - \exp\{-(\mu/\rho) \times (d_c)(\rho_{stp})(\phi/760)\}$ missing number implies unit value.

[b] Reference 9.

[c] μ/ρ values for carbon, magnesium, and aluminum are estimated from *Handbook of Chemistry and Physics* (Chemical Rubber Publishing Company, Cleveland, Ohio, 1958), 42nd ed.

[d] ω_K values for carbon, magnesium, and aluminum are estimated from Refs. 10–13.

TABLE II. L-shell ionization cross sections.

Element	Z	E_p (keV)	$N(E_p)$ (x rays/μC)	$\frac{A^a}{T_w A_c}$	I_μ (x rays/ proton)	$\frac{dI_\mu}{dE_p}$ (x rays/ proton-keV)	$S(E)^b$ (keV-cm^2/ mg)	$\frac{1}{n}\frac{dI_\mu}{dE_p}S(E)$	$\frac{1}{n}\frac{\mu}{\rho}I_\mu{}^c$	σ_x (cm^2)	σI^d (cm^2)
Neodymium	60	500	3200	$\frac{46\,090}{(0.97)_w(0.97)_c}$	2.4(−5)	1.8(−7)	95	4.2(−24)	1.5(−24)	5.7(−24)	2.8(−23)
L shell		700	12 000	$\frac{46\,090}{(0.97)_w(0.97)_c}$	8.9(−5)	4.8(−7)	85	9.8(−24)	5.7(−24)	1.5(−23)	7.8(−23)
$h\nu \approx 5.2$ keV		900	30 000	$\frac{46\,090}{(0.97)_w(0.97)_c}$	2.3(−4)	9.7(−7)	75	1.7(−23)	1.5(−23)	3.2(−23)	1.6(−22)
$\mu/\rho = 270$ cm^2/gm		1100	57 000	$\frac{46\,090}{(0.97)_w(0.97)_c}$	4.5(−4)	1.3(−6)	68	2.1(−23)	2.9(−23)	5.0(−23)	2.5(−22)
		1300	97 000	$\frac{46\,090}{(0.97)_w(0.97)_c}$	7.5(−4)	1.7(−6)	62	2.6(−23)	4.8(−23)	7.4(−23)	3.7(−22)
$\omega_L = 0.20$		1500	140 000	$\frac{46\,090}{(0.97)_w(0.97)_c}$	1.1(−3)	2.1(−6)	55	2.7(−23)	7.2(−23)	1.0(−22)	5.0(−22)
		1700	200 000	$\frac{46\,090}{(0.97)_w(0.97)_c}$	1.6(−3)	2.3(−6)	51	2.8(−23)	1.0(−22)	1.3(−22)	6.4(−22)
Samarium	62	500	2 300	$\frac{46\,090}{(0.99)_w(0.96)_c}$	1.8(−5)	1.5(−7)	95	3.7(−24)	1.1(−24)	4.8(−24)	2.3(−23)
L shell		700	9 100	$\frac{46\,090}{(0.99)_w(0.96)_c}$	7.2(−5)	4.0(−7)	85	8.5(−24)	4.3(−24)	1.3(−23)	6.4(−23)
$h\nu \approx 5.6$ keV		900	23 000	$\frac{46\,090}{(0.99)_w(0.96)_c}$	1.8(−4)	7.3(−7)	75	1.4(−23)	1.1(−23)	2.5(−23)	1.2(−22)
$\mu/\rho = 240$ cm^2/gm		1100	46 000	$\frac{46\,090}{(0.99)_w(0.96)_c}$	3.6(−4)	1.0(−6)	68	1.7(−23)	2.2(−23)	3.9(−23)	2.0(−22)
		1300	79 000	$\frac{46\,090}{(0.99)_w(0.96)_c}$	5.9(−4)	1.4(−6)	62	2.1(−23)	3.6(−23)	5.7(−23)	2.8(−22)
$\omega_L = 0.20$		1500	120 000	$\frac{46\,090}{(0.99)_w(0.96)_c}$	9.0(−4)	1.8(−6)	55	2.4(−23)	5.5(−23)	7.9(−23)	4.0(−22)
		1700	170 000	$\frac{46\,090}{(0.99)_w(0.96)_c}$	1.3(−3)	2.2(−6)	51	2.8(−23)	7.9(−23)	1.1(−22)	5.3(−22)
Gadolinium	64	500	1 700	$\frac{46\,090}{(1)_w(0.93)_c}$	1.4(−5)	1.4(−7)	95	3.4(−24)	8.1(−25)	4.2(−24)	2.1(−23)
L shell		700	7 100	$\frac{46\,090}{(1)_w(0.93)_c}$	5.7(−5)	3.2(−7)	85	7.0(−24)	3.3(−24)	1.0(−23)	5.2(−23)
$h\nu \approx 6.1$		900	18 000	$\frac{46\,090}{(1)_w(0.93)_c}$	1.5(−4)	6.0(−7)	75	1.2(−23)	8.6(−24)	2.0(−23)	1.0(−22)
$\mu/\rho = 220$ cm^2/gm		1100	36 000	$\frac{46\,090}{(1)_w(0.93)_c}$	2.9(−4)	8.5(−7)	68	1.5(−23)	1.7(−23)	3.2(−23)	1.6(−22)
		1300	61 000	$\frac{46\,090}{(1)_w(0.93)_c}$	4.9(−4)	1.1(−6)	62	1.8(−23)	2.8(−23)	4.6(−23)	2.3(−22)
$\omega_L = 0.20$		1500	91 000	$\frac{46\,090}{(1)_w(0.93)_c}$	7.2(−4)	1.3(−6)	55	1.9(−23)	4.2(−23)	6.1(−23)	3.0(−22)
		1700	130 000	$\frac{46\,090}{(1)_w(0.93)_c}$	1.0(−3)	1.6(−6)	51	2.2(−23)	5.9(−23)	8.0(−23)	4.0(−22)

amplifier; voltage pulses higher than those of interest are excluded with the upper setting of the discriminator window. Owing to drifts in the circuit the discriminator window may drift relative to the voltage pulse and thereby disturb the count rate. Monitoring of this window selection is performed using a 400-channel pulse-height analyzer. The scaler collects counts for a period corresponding to the time required to collect a predetermined charge, i.e., the scaler is gated by a current integrator. The current integrator is calibrated to better than 5% using a constant current source. A standard check was to pulse the counting circuit with a known frequency (0–10 kc/sec) and pulse height at the input to the preamplifier. The response of the scaler was within 1%. The counting gas was selected to satisfy two conditions: distribute the x-ray absorption over a reasonable (>20%) portion of the counter diameter and reduce high-energy background. It has been found that absorption of the radiation too near the window (<2% of counter diameter) distorted the symmetrical shape of the observed spectrum and reduced the counter efficiency. For the carbon measurements a 96% helium plus 4% isobutane mixture was employed at 20-cm Hg pressure. This made the counter diameter (2 in.) the equivalent of one absorption length for the x rays. The helium mixture was also used in the M-shell measurements to reduce counter absorption of the intense L-shell radiation at proton energies above 1 MeV. For all other measurements the standard 90% argon plus 10% methane mixture[7] was used.

[7] P-10 supplied by Matheson Company.

TABLE II (*continued*)

Element	Z	E_p (keV)	$N(E_p)$ (x rays/μC)	$\frac{A^a}{T_w A_c}$	I_μ (x rays/ proton)	$\frac{dI_\mu}{dE_p}$ (x rays/ proton-keV)	$S(E)^b$ (keV-cm^2/ mg)	$\frac{1}{n}\frac{dI_\mu}{dE_p}S(E)$	$\frac{1}{n\rho}\mu I_\mu{}^c$	σ_x (cm^2)	$\sigma_I{}^d$ (cm^2)
Terbium	65	500	1 400	$\frac{46\,090}{(1)_w(0.90)_c}$	1.1(−5)	1.0(−7)	95	2.6(−24)	6.6(−25)	3.3(−24)	1.6(−23)
L shell		700	6 000	$\frac{46\,090}{(1)_w(0.90)_c}$	5.0(−5)	2.8(−7)	85	6.3(−24)	2.9(−24)	9.2(−24)	4.6(−23)
$h\nu \approx 6.3$ keV		900	16 000	$\frac{46\,090}{(1)_w(0.90)_c}$	1.3(−4)	5.4(−7)	75	1.1(−23)	7.6(−24)	1.8(−23)	9.2(−23)
$\mu/\rho = 220$ cm^2/gm		1100	32 000	$\frac{46\,090}{(1)_w(0.90)_c}$	2.6(−4)	8.0(−7)	68	1.4(−23)	1.5(−23)	2.9(−23)	1.5(−22)
		1300	55 000	$\frac{46\,090}{(1)_w(0.90)_c}$	4.4(−4)	1.0(−6)	62	1.7(−23)	2.6(−23)	4.2(−23)	2.1(−22)
$\omega_L = 0.20$		1500	83 000	$\frac{46\,090}{(1)_w(0.90)_c}$	6.7(−4)	1.3(−6)	55	1.9(−23)	3.9(−23)	5.8(−23)	2.9(−22)
		1700	120 000	$\frac{46\,090}{(1)_w(0.90)_c}$	9.7(−4)	1.7(−6)	51	2.2(−23)	5.6(−23)	7.9(−23)	3.9(−22)
Dysprosium	66	500	1200	$\frac{46\,090}{(1)_w(0.88)_c}$	1.0(−5)	9.2(−8)	95	2.4(−24)	5.5(−25)	2.9(−24)	1.5(−23)
L shell		700	5100	$\frac{46\,090}{(1)_w(0.88)_c}$	4.4(−5)	2.5(−7)	85	5.8(−24)	2.4(−24)	8.3(−24)	4.1(−23)
$h\nu \approx 6.5$ keV		900	13 000	$\frac{46\,090}{(1)_w(0.88)_c}$	1.1(−4)	4.7(−7)	75	9.5(−24)	6.3(−24)	1.6(−23)	7.9(−23)
$\mu/\rho = 200$ cm^2/gm		1100	27 000	$\frac{46\,090}{(1)_w(0.88)_c}$	2.3(−4)	7.2(−7)	68	1.3(−23)	1.3(−23)	2.6(−23)	1.3(−22)
		1300	47 000	$\frac{46\,090}{(1)_w(0.88)_c}$	4.0(−4)	9.5(−7)	62	1.6(−23)	2.2(−23)	3.8(−23)	1.9(−22)
$\omega_L = 0.20$		1500	73 000	$\frac{46\,090}{(1)_w(0.88)_c}$	6.1(−4)	1.2(−6)	55	1.8(−23)	3.3(−23)	5.2(−23)	2.6(−22)
		1700	100 000	$\frac{46\,090}{(1)_w(0.88)_c}$	8.9(−4)	1.6(−6)	51	2.1(−23)	4.9(−23)	7.0(−23)	3.5(−22)
Holmium	67	500	980	$\frac{46\,090}{(1)_w(0.83)_c}$	8.8(−6)	8.8(−8)	95	2.3(−24)	4.7(−25)	2.8(−24)	1.4(−23)
L shell		700	4400	$\frac{46\,090}{(1)_w(0.83)_c}$	3.8(−5)	2.1(−7)	85	5.0(−24)	2.0(−24)	7.0(−24)	3.5(−23)
$h\nu \approx 6.7$ keV		900	12 000	$\frac{46\,090}{(1)_w(0.83)_c}$	1.0(−4)	4.3(−7)	75	8.8(−24)	5.4(−24)	1.4(−23)	7.1(−23)
$\mu/\rho = 200$ cm^2/gm		1100	23 000	$\frac{46\,090}{(1)_w(0.83)_c}$	2.1(−4)	6.7(−7)	68	1.2(−23)	1.1(−23)	2.4(−23)	1.2(−22)
		1300	40 000	$\frac{46\,090}{(1)_w(0.83)_c}$	3.7(−4)	8.7(−7)	62	1.5(−23)	2.0(−23)	3.5(−23)	1.7(−22)
$\omega_L = 0.20$		1500	65 000	$\frac{46\,090}{(1)_w(0.83)_c}$	5.7(−4)	1.1(−6)	55	1.7(−23)	3.0(−23)	4.7(−23)	2.4(−22)
		1700	92 000	$\frac{46\,090}{(1)_w(0.83)_c}$	8.1(−4)	1.4(−6)	51	1.9(−23)	4.4(−23)	6.3(−23)	3.1(−24)

[a] See footnote a, Table I.
[b] See footnote b, Table I.
[c] μ/ρ values estimated from Refs. 14 and Handbook of Chemistry and Physics (Chemical Rubber Publishing Company, Cleveland, Ohio, 1958), 42nd ed.
[d] ω_L values estimated from Ref. 10 and Hans Mark (private communication).

The counter window materials were selected to transmit the soft x rays and to supply a conducting surface to make the proportional counter field more uniform. For the carbon measurement 0.25-mil aluminized Mylar was used (5% transmission). One-mil beryllium was used for the L- and M-shell studies and 0.4-mil aluminum foil was used for all others. The transmissions of all foils were measured directly. The counter efficiencies were established by counter pressure variation techniques.

At energies above 1 MeV it was found that scattered protons would penetrate the foils and produce a large background signal in the counter. To reduce this effect, an 18-in. extension was placed between the target chamber and the counter. Two magnetron magnets were located in this extension to deflect the protons from the counter window.

For all experiments the counter signal-to-noise ratio was no less than 10:1 but was normally maintained at better than 100:1. Counter background was of the order of 1 cps. A potential source of error in the yield measurements, particularly important at low bombarding energies, originates from the formation of a carbonaceous contaminant on the surface of the target. This effect has been discussed elsewhere.[1] A detailed investigation of target contamination has been made possible by the ability to observe the carbon x rays. The results of this study are included as an appendix.

TABLE III. M-shell ionization cross sections.

Element	Z	E_p (keV)	$N(E_p)$ (x rays/μC)	$\frac{\Delta^a}{T_w A_c}$	I_μ (x rays/ proton)	$\frac{dI_\mu}{dE_p}$ (x rays/ proton-keV)	$S(E)^b$ (keV-cm^2/ mg)	$\frac{1}{n}\frac{dI_\mu}{dE_p}S(E)$	$\frac{1}{n}\frac{\mu}{\rho}I_\mu{}^c$	σ_x (cm^2)	$\sigma_I{}^d$ (cm^2)
Neodymium	60	500	1700	$\frac{46\,090}{(0.08)_w}$	1.6(−4)	6.3(−7)	95	1.4(−23)	6.7(−23)	8.1(−23)	8.1(−21)
M shell		700	3100	$\frac{46\,090}{(0.08)_w}$	2.8(−4)	6.3(−7)	85	1.3(−23)	1.2(−22)	1.3(−22)	1.3(−20)
$h\nu \approx 0.98$ keV		900	4700	$\frac{46\,090}{(0.08)_w}$	4.1(−4)	6.3(−7)	75	1.1(−23)	1.7(−22)	1.8(−22)	1.8(−20)
$\mu/\rho = 1700$ cm^2/gm		1100	6100	$\frac{46\,090}{(0.08)_w}$	5.4(−4)	5.9(−7)	68	9.6(−24)	2.3(−22)	2.4(−22)	2.4(−20)
		1300	7300	$\frac{46\,090}{(0.08)_w}$	6.4(−4)	5.4(−7)	62	8.1(−24)	2.7(−22)	2.8(−22)	2.8(−20)
$\omega_M = 0.01$		1500	8500	$\frac{46\,090}{(0.08)_w}$	7.5(−4)	4.7(−7)	55	6.2(−24)	3.1(−22)	3.2(−22)	3.2(−20)
		1700	9600	$\frac{46\,090}{(0.08)_w}$	8.4(−4)	3.8(−7)	51	4.7(−24)	3.5(−22)	3.6(−22)	3.6(−20)
Samarium	62	500	3700	$\frac{46\,090}{(0.13)_w}$	1.8(−4)	6.8(−7)	95	1.6(−23)	6.9(−23)	8.5(−23)	8.5(−21)
M shell		700	5700	$\frac{46\,090}{(0.13)_w}$	3.2(−4)	6.8(−7)	85	1.4(−23)	1.2(−22)	1.3(−22)	1.3(−20)
$h\nu \approx 1.1$ keV		900	8100	$\frac{46\,090}{(0.13)_w}$	4.6(−4)	6.7(−7)	75	1.2(−23)	1.7(−22)	1.8(−22)	1.8(−20)
$\mu/\rho = 1500$ cm^2/gm		1100	11 000	$\frac{46\,090}{(0.13)_w}$	5.8(−4)	6.1(−7)	68	1.0(−23)	2.2(−22)	2.3(−22)	2.3(−20)
		1300	13 000	$\frac{46\,090}{(0.13)_w}$	7.0(−4)	5.5(−7)	62	8.0(−24)	2.6(−22)	2.7(−22)	2.7(−20)
$\omega_M = 0.01$		1500	15 000	$\frac{46\,090}{(0.13)_w}$	8.0(−4)	4.7(−7)	55	6.0(−24)	3.0(−22)	3.1(−22)	3.1(−20)
		1700	16 000	$\frac{46\,090}{(0.13)_w}$	8.8(−4)	3.4(−7)	51	4.0(−24)	3.3(−22)	3.4(−22)	3.4(−20)
Gadolinium	64	500	6300	$\frac{46\,090}{(0.19)_w}$	2.6(−4)	8.9(−7)	95	2.2(−23)	9.1(−23)	1.1(−22)	1.1(−20)
M shell		700	10 000	$\frac{46\,090}{(0.19)_w}$	4.4(−4)	8.9(−7)	85	2.0(−23)	1.5(−22)	1.7(−22)	1.7(−20)
$h\nu \approx 1.2$ keV		900	15 000	$\frac{46\,090}{(0.19)_w}$	6.2(−4)	8.8(−7)	75	1.7(−23)	2.2(−22)	2.3(−22)	2.3(−20)
$\mu/\rho = 1300$ cm^2/gm		1100	19 000	$\frac{46\,090}{(0.19)_w}$	7.9(−4)	8.1(−7)	68	1.4(−23)	2.8(−22)	2.9(−22)	2.9(−20)
		1300	23 000	$\frac{46\,090}{(0.19)_w}$	9.5(−4)	7.3(−7)	62	1.2(−23)	3.3(−22)	3.2(−22)	3.2(−20)
$\omega_M = 0.01$		1500	26 000	$\frac{46\,090}{(0.19)_w}$	1.1(−3)	6.3(−7)	55	1.0(−23)	3.8(−22)	3.9(−22)	3.9(−20)
		1700	28 000	$\frac{46\,090}{(0.19)_w}$	1.2(−3)	4.8(−7)	51	1.0(−23)	4.2(−22)	4.3(−22)	4.3(−20)

CROSS-SECTION CALCULATIONS

The directly measured quantity in these experiments was $N(E_p)$, i.e., the number of x rays per μC before correction for geometry, window absorption, and detection efficiency. After corrections have been made the thick target yield I_μ (x rays per proton) is obtained. The x-ray production cross section is calculated by the formula[3,8]:

$$\sigma_x = \frac{1}{n}\left[\frac{dI_\mu}{dE_p}S(E_p) + \frac{\mu}{\rho}I_\mu\right]. \quad (1)$$

To correct for Auger processes it is necessary to know the fluorescence yield ω for the shell and element. The ionization cross section is then given by

$$\sigma_I = \sigma_x/\omega.$$

In Eq. (1) n is the number of target atoms per gram, $S(E_p)$ is the stopping power, and μ/ρ is the self-absorption coefficient. With known values for these quantities and ω, the calculation is quite straightforward. It is at this point, however, that the largest uncertainties exist. There are few values of the stopping power below 100 keV and then only for a limited number of elements.[9] It is necessary then to extrapolate in energy and interpolate in Z to obtain usable numbers. The mass absorption coefficients are similarly imprecisely known for the heavier elements. The largest un-

[8] H. W. Lewis, B. E. Simmons, and E. Merzbacher, Phys. Rev. **91**, 943 (1953).

[9] S. D. Warshaw and S. K. Allison, Rev. Mod. Phys. **25**, 779 (1953).

TABLE III (*continued*)

Element	Z	E_p (keV)	$N(E_p)$ (x rays/μC)	$\frac{A^a}{T_w A_c}$	I_μ (x rays/ proton)	$\frac{dI_\mu}{dE_p}$ (x rays/ proton-keV)	$S(E)^b$ (keV-cm^2/ mg)	$\frac{1}{n}\frac{dI_\mu}{dE_p}S(E)$	$\frac{1}{n\rho}I_\mu{}^c$	σ_x (cm^2)	σI^d (cm^2)
Terbium	65	500	7800	$\frac{46\,090}{(0.20)_w}$	2.8(−4)	9.8(−7)	95	2.5(−23)	9.5(−23)	1.2(−22)	1.2(−20)
M shell		700	13 000	$\frac{46\,090}{(0.20)_w}$	4.7(−4)	9.8(−7)	85	2.2(−23)	1.6(−22)	1.8(−22)	1.8(−20)
$h\nu \approx 1.2$ keV		900	19 000	$\frac{46\,090}{(0.20)_w}$	6.6(−4)	9.6(−7)	75	1.9(−23)	2.3(−22)	2.5(−22)	2.5(−20)
$\mu/\rho = 1300$ cm^2/gm		1100	24 000	$\frac{46\,090}{(0.20)_w}$	8.5(−4)	8.8(−7)	68	1.6(−23)	2.9(−22)	3.1(−22)	3.1(−20)
		1300	29 000	$\frac{46\,090}{(0.20)_w}$	1.0(−3)	7.8(−7)	62	1.0(−23)	3.5(−22)	3.6(−22)	3.6(−20)
$\omega_M = 0.01$		1500	33 000	$\frac{46\,090}{(0.20)_w}$	1.2(−3)	6.4(−7)	55	1.0(−23)	4.0(−22)	4.1(−22)	4.1(−20)
		1700	36 000	$\frac{46\,090}{(0.20)_w}$	1.3(−3)	5.0(−7)	51	1.0(−23)	4.4(−22)	4.5(−22)	4.5(−20)
Dysprosium	66	500	9400	$\frac{46\,090}{(0.24)_w}$	2.9(−4)	1.0(−6)	95	2.7(−23)	1.0(−22)	1.3(−22)	1.3(−20)
M shell		700	16 000	$\frac{46\,090}{(0.24)_w}$	5.0(−4)	1.0(−6)	85	2.4(−23)	1.7(−22)	2.0(−22)	2.0(−20)
$h\nu \approx 1.3$ keV		900	23 000	$\frac{46\,090}{(0.24)_w}$	7.1(−4)	1.0(−6)	75	2.1(−23)	2.4(−22)	2.6(−22)	2.6(−20)
$\mu/\rho = 1270$ cm^2/gm		1100	25 000	$\frac{46\,090}{(0.24)_w}$	9.1(−4)	9.4(−7)	68	2.0(−23)	3.1(−22)	3.3(−22)	3.3(−20)
		1300	35 000	$\frac{46\,090}{(0.24)_w}$	1.1(−3)	8.4(−7)	62	1.0(−23)	3.7(−22)	3.8(−22)	3.8(−20)
$\omega_M = 0.01$		1500	40 000	$\frac{46\,090}{(0.24)_w}$	1.2(−3)	7.2(−7)	55	1.0(−23)	4.3(−22)	4.4(−22)	4.4(−20)
		1700	44 000	$\frac{46\,090}{(0.24)_w}$	1.4(−3)	5.7(−7)	51	1.0(−23)	4.7(−22)	4.8(−22)	4.8(−20)
Holmium	67	500	12 000	$\frac{46\,090}{(0.27)_w}$	3.3(−4)	1.2(−6)	95	3.1(−23)	1.2(−22)	1.5(−22)	1.5(−20)
M shell		700	21 000	$\frac{46\,090}{(0.27)_w}$	5.7(−4)	1.2(−6)	85	2.8(−23)	2.0(−22)	2.3(−22)	2.3(−20)
$h\nu \approx 1.35$ keV		900	30 000	$\frac{46\,090}{(0.27)_w}$	8.0(−4)	1.2(−6)	75	2.4(−23)	2.8(−22)	3.0(−22)	3.0(−20
$\mu/\rho = 1270$ cm^2/gm		1100	37 000	$\frac{46\,090}{(0.27)_w}$	1.0(−3)	1.1(−6)	68	2.0(−23)	3.6(−22)	3.8(−22)	3.8(−20)
		1300	45 000	$\frac{46\,090}{(0.27)_w}$	1.2(−3)	9.8(−7)	62	2.0(−23)	4.3(−22)	4.5(−22)	4.5(−20)
$\omega_M = 0.01$		1500	52 000	$\frac{46\,090}{(0.27)_w}$	1.4(−3)	8.2(−7)	55	1.0(−23)	5.0(−22)	5.1(−22)	5.1(−20)
		1700	57 000	$\frac{46\,090}{(0.27)_w}$	1.6(−3)	6.6(−7)	51	1.0(−23)	5.5(−22)	5.6(−22)	5.6(−20

[a] See footnote a, Table I.
[b] See footnote b, Table I.
[c] Source of μ/ρ values Ref. 14.
[d] ω_M values estimated by Hans Mark (private communication).

certainty resides in the values of the fluorescence yields. All values employed in this paper are either extrapolations of considerable extent or experimental values of questionable validity.[10] As a result of the foregoing considerations the calculations for each energy are tabulated so that corrections may be easily made or uncertainties in cross sections quickly estimated from the corresponding support data uncertainty.

Table I contains the K-shell results for carbon, magnesium, and aluminum in the ranges 15–110 keV and 500–1900 keV. Of these elements the ionization cross section of aluminum are the most reliable. Allison and Warshaw[9] show values for the stopping power down to 50 keV, from which lower extrapolation is easily made. The self-absorption coefficient μ/ρ is readily measured and is established to within a few percent. The fluorescence yield value for aluminum remains somewhat questionable. There are three experimental values: 0.008±0.003 (Ref. 11), 0.038±0.015 (Ref. 12), and 0.045±0.002 (Ref. 13). The authors

[10] E. H. S. Burhop, *The Auger Effect and Other Radiationless Transitions* (Cambridge University Press, Cambridge, England, 1952).

[11] R. A. Rightmire, J. R. Simauton, and T. P. Kohman, Phys. Rev. **113**, 1069 (1957).

[12] A. A. Konstantinov, V. V. Perepelkin, and T. E. Sazonova, Izv. Akad. Nauk SSSR, Ser. Fiz. **28**, 107 (1964) [Colombia Tech. Transl. **28**, 103 (1964)].

[13] F. Bertrand, G. Charpak, and F. Suzor, J. Phys. Radium **20**, 463, 956 (1959).

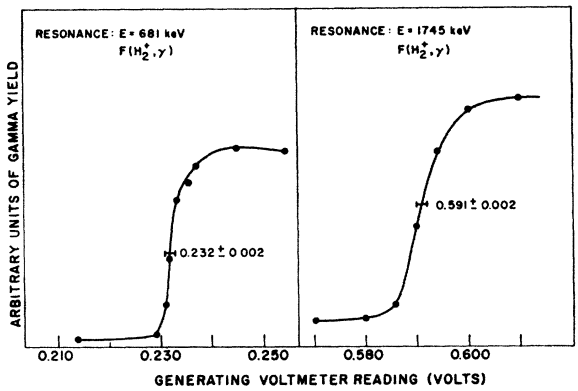

FIG. 1. Fluorine resonances used to calibrate Van de Graaff generator.

have chosen a value of 0.029. For Mg and C the values of the stopping power were obtained by interpolation between the values shown by Allison and Warshaw.[9] The values are certainly valid to within ±30%. The absorption coefficients for these elements are available. Again, the fluorescence yield values are but a plausible extrapolation.

Table II contains the L-shell cross sections over the energy range 500–1700 keV for six rare-earth elements ranging from $Z=60$ to 67. Owing to the small spread in Z covered, similar values of the stopping power and fluorescence yield (0.20) were used for all elements. This clearly introduces a systematic error. Extrapolated values for the self-absorption coefficient were used.[14]

Table III contains the M-shell values over the two energy ranges 25–100 keV and 500–1700 keV. The ionization cross sections for these elements in the M shell are least accurately known. Stopping powers are within 30% at energies above 200 keV. Below this energy the errors may be as much as twice as large. The self-absorption coefficient is ±30%. The fluorescence yield must be considered only an order of magnitude estimate.

To review the errors in the tabulated values the following assignment is made: I_μ: ±15%, σ_x: ±30%, σ_I to within a factor of 3. The aluminum σ_x is somewhat better known but the σ_I is within the above error. The M-shell values are consistent with the above assignment, excluding σ_I, which must be an order of magnitude number reflecting the fluorescence yield uncertainty.

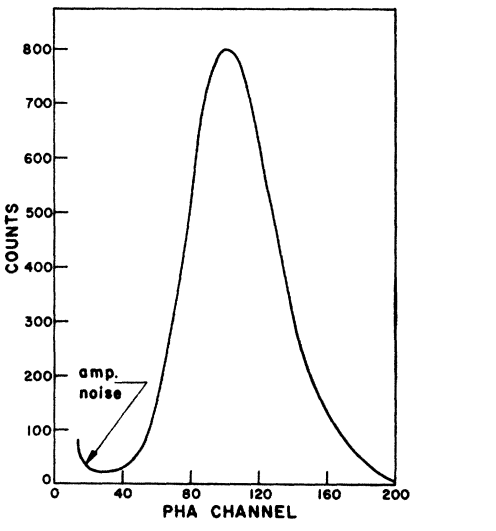

FIG. 2. Typical (aluminum) pulse-height analyses of proportional-counter output spectrum.

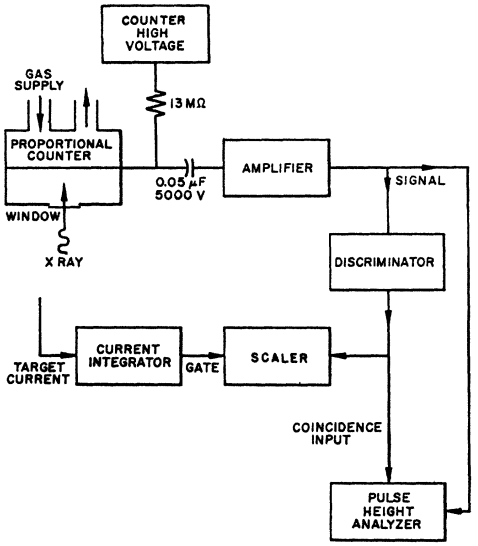

FIG. 3. Proportional-counter circuit.

SUMMARY

It is clear from the preceding remarks that the ionization cross sections obtained have a number of uncertainties that are unavoidable at the moment. Even in this context interesting points present themselves. These are primarily associated with the K-shell results and will be given below. In view of the orders of magnitude over which the data spread, graphical presentation is employed, including any previous data available.

The K-shell data present a most interesting set for comparison with theoretical prediction. Carbon is the lowest Z material with the lowest K-shell binding energy (283 eV) to be studied by the authors. As a result of the low binding energy the predicted peaking of the cross section is brought within the range of the current experiment. The peak occurs at about 500 keV and is very broad. (Figure 4 shows peaking in the thick target yield.) Plotted in Fig. 5 along with the experimental data are the results of a numerical evaluation of the Born-approximation expression as presented by Merz-

[14] A. H. Compton and S. K. Allison, *X-Rays in Theory and Practice* (D. Van Nostrand Company, Inc., Princeton, New Jersey, 1960).

bacher and Lewis.[3] The two peak at roughly the same point. The factor of 2 difference may not be significant in view of the uncertainty in the fluorescence yield employed (0.007). As the proton energy is decreased the cross section drops away from the predicted as one might expect from a breakdown of the assumptions implicit in the Born approximation. A proposed alternative at lower energies would be the semiclassical description of Bang and Hansteen. These values for C have not been calculated by the authors.

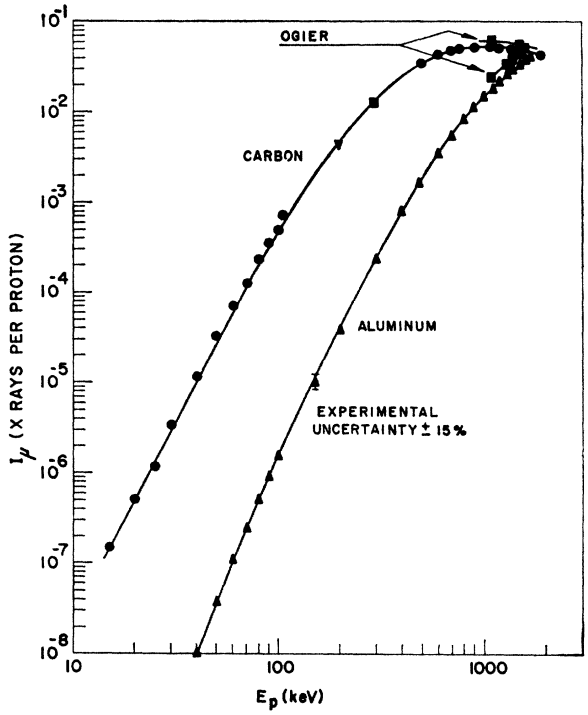

FIG. 4. K-shell thick-target yield for carbon and aluminum. Values measured by Ogier (private communication) using cyclotron with internal target.

The K-shell results for aluminum over the range from 25 to 1700 keV are presented in Fig. 6. Over this range of proton energy the cross section is monotonically increasing. Shown in the same figure are the Born approximation results. They appear to cross the experimental results at 600 keV but this is a result of the fluorescence yield chosen (0.029). The flags on the experimental data reflect the spread in measured fluorescence yields. The chosen value lies near the mean. Also presented in Fig. 6 are the results based upon the Bang and Hansteen calculation. To be more specific the Born approximation describes the proton by use of a plane wave while Bang and Hansteen assign a classical hyperbolic trajectory to the proton. As it is believed that the ionizing interaction takes place at an impact parameter approximately the radius of the shell (and therefore large compared with the distance of closest approach), it can be shown that the proton may

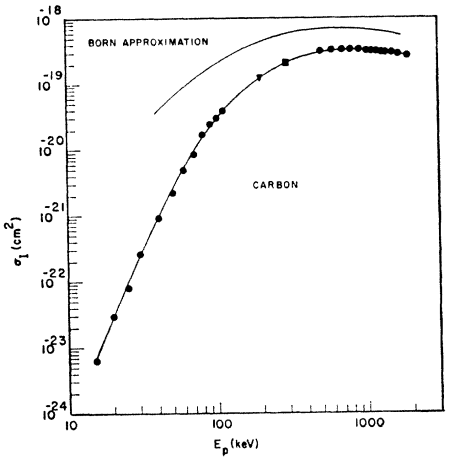

FIG. 5. K-shell ionization cross section for carbon, experimental and Born approximation.

be treated classically. Thus the Bang and Hansteen formulation is of particular interest. It must be remarked, however, that the evaluation of the particular expressions [Eq. (3.28) and following equations of Ref. 5] is considered valid in the range $d\alpha<\alpha/q_0\ll 1$ where d is the distance of closest approach, $1/\alpha$ is the Bohr radius, and q_0 is the minimum momentum transfer by the proton. For aluminum at proton energies from 25 to 300 keV the ratio α/q_0 varies from 0.2 to 0.8. The curve shown may reflect the gradual breakdown of the assumptions. Work is currently in progress to remove these particular restrictions. However, it is not expected to effect the values at lower E_p appreciably.

The L- and M-shell results are presented in Fig. 7 and show fairly regular features. L-shell Born approximation values are shown for holmium and are in reasonable agreement with the data. Neodymium is shown to indicate the spread in values as Z varies from 60 to 67.

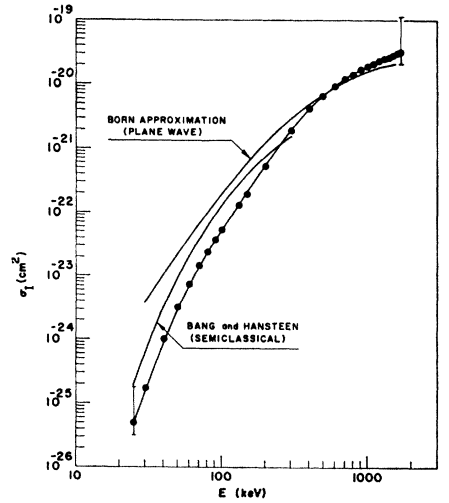

FIG. 6. K-shell ionization cross section for aluminum, experimental, Born approximation, and semiclassical.

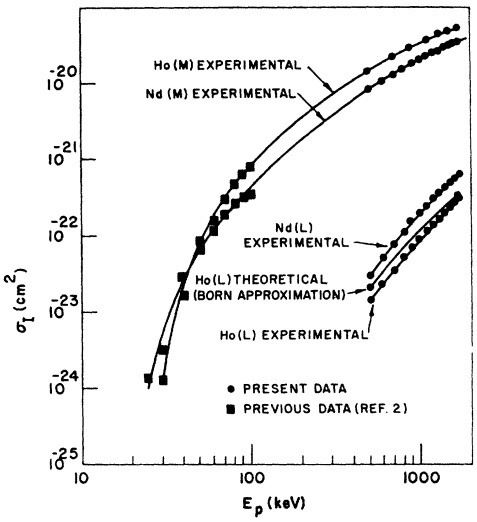

FIG. 7. L- and M-shell ionization cross sections for Nd and Ho, experimental and Born approximation (L only).

There are at present no theoretical results available for comparison with the M-shell results given in Fig. 7. The apparent crossing of the two curves may well reflect the uncertainties in absorption cross section, stopping power, and fluorescence yield, and is not considered significant by the authors.

APPENDIX: CONTAMINATION STUDY

At low bombarding energies target surface contamination has generally been a serious concern, having the effect of reducing the energy of the beam particles.[1] The term contamination implies addition of material different than the target. On the basis of the current experiment, it is felt that most (>90%) of the usually observed contamination is carbon. This was demonstrated by two experiments. A carbon target was bombarded for several hours at 5-μA current. The carbon x-ray yield stayed constant to within $\pm 5\%$. Under similar conditions, a copper target was placed in the beam and carbon x rays were observed. The carbon yield doubled in 12 min (at 60 keV) and appeared to be increasing linearly in time. After 20 min the copper x-ray yield (simultaneously observed) started to decrease, corresponding to an energy loss in the carbon film of over 1 keV. A flaw in the reasoning might lie in the existence of some other contaminant with an x-ray line indistinguishable from carbon and having the same x-ray production cross section over the energy range from 15 to 110 keV. This seems most unlikely. By employing the x-ray production cross section the surface density of carbon (atoms/cm^2) is presented as a function of time and beam current. The dependence of rate upon current has been empirically fit by a curve. This empirical relation lends itself to physical interpretation in terms of the residence time and impingement rate of decomposable hydrocarbons upon the surface. The generalization has not yet been given a series of rigorous tests, but may be useful as a starting point for further investigation.

Experimental Arrangement

The experimental apparatus employed to make the contamination measurements is the same as was used for the carbon yield measurements. The principal addition was that two separate differential discriminator-scaler systems were employed to simultaneously record the counts from both the copper and carbon x rays. Both scaler systems were gated on the output of a current integrator to turn off at a preset charge. As was the case during the carbon yield measurement, the proportional counter was operated in a flow mode at a reduced pressure. Therefore, the carbon counts can be considered as absolute yield numbers. At the reduced pressures only a small fraction of the copper L x rays are stopped within the counter. (Although only copper is referred to in the work, tests showed that the results were qualitatively the same for an aluminum target.)

The purpose of monitoring the copper yield was to test for change in energy of the proton beam. In the 30- to 100-keV region, a 1-keV change in energy of the protons would result in at least 10% change in the copper yield. During the course of the contamination studies, the contaminant thickness was such that less than 1 keV was lost. This defines a truly thin target condition for the contaminant.

The vacuum environment of the target has a direct bearing upon the results. During the course of the experiments the pressure, measured 12 in. from the target, was 1.2×10^{-6} mm Hg. This gauge was in close proximity to a cold trap. Therefore, information regarding the condensible component of the gas impinging upon the target was largely lost. However, the value of the work presented here is twofold—to indicate typical values for contamination buildup and to propose a functional relationship that might describe the process. With this relationship as a starting point further tests might be performed under more controlled conditions.

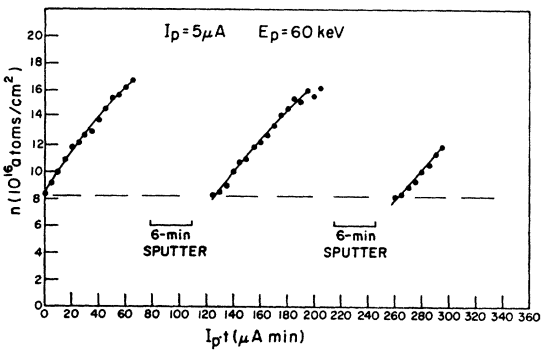

FIG. 8. Sputter cleaning of copper target.

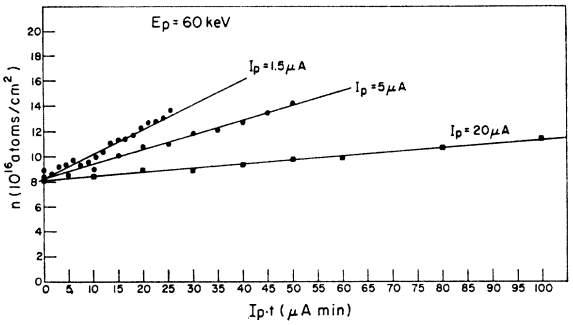

FIG. 9. Contamination buildup—I.

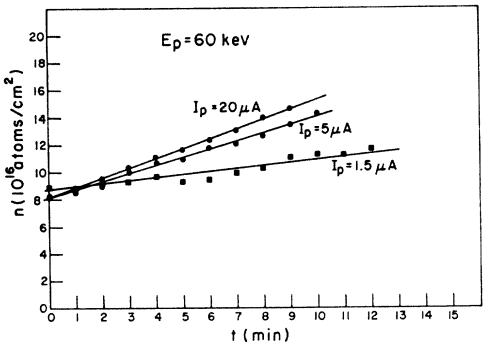

FIG. 10. Contamination buildup—II.

Data

The contamination measurements are presented in Figs. 8 through 11. The ordinate in all cases is in units of 10^{16} atoms of carbon per cm^2. This number is derived in the following manner. The observed counts (corrected for geometry and window and counter absorptions) are measured as x rays per proton (I_μ). Under the thin-target conditions,

$$I_\mu = n(\text{atoms/cm}^2)\sigma_x(\text{cm}^2/\text{atom}).$$

The values for the x-ray production cross section are taken from Table I. The equation is solved for n.

Sputter Cleaning

In Fig. 8, the carbon thickness versus time is presented during a series of bombardment and cleaning cycles at 60 keV with a proton current of 5 μA. The sputtering was performed at 100 μHg pressure of argon gas (600 V, 5 mA) for 6 min. It is interesting to note that the contamination rate and the base line remained constant.

Contamination Rates

In Figs. 9 and 10 the carbon buildup is plotted against μA-min (or protons onto target) and against time. It is clear that in neither case are the slopes for the three proton currents the same. This implies that in this range it is neither simply a conversion process actuated by the protons nor purely a surface decomposition of incident hydrocarbons.

Energy Dependence

In Figs. 11 are shown two sets of contamination buildups covering 30, 60, and 100 keV. Each set was

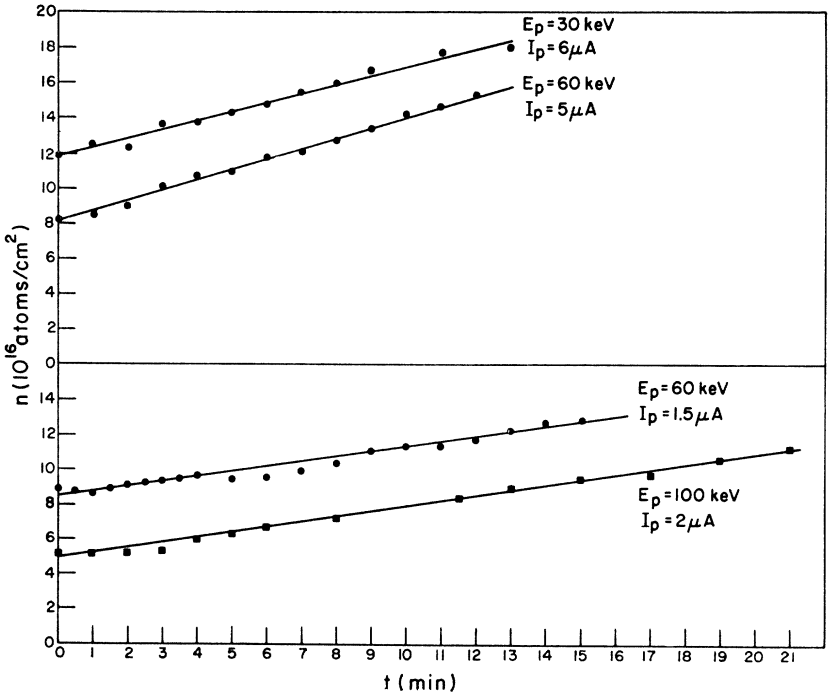

FIG. 11. Energy independence of contamination buildup.

measured at essentially the same proton current, showing that the contamination rate is largely independent of proton energy.

Surface cleaning is a subject of some interest. The values shown in Figs. 8 through 11 were taken as reproducible values following 6-min sputter cleanings; however, it was found that values of the base line at $E_p=60$ keV lower than 8×10^{16} atoms/cm^2 could be obtained when the sanding and polishing was followed by sputtering. This improvement represented only a 20% decrease and was not wholly reproducible.

Interpretation

From the data represented by Figs. 9 and 10 it is possible to construct an empirical relation which contains the buildup dependence upon proton current and time. The expression obtained was

$$n=n_0+0.7\times10^{16}[1-\exp(-0.35I_p)]t,$$

where n is carbon atoms/cm^2, I_p is measured in μA/cm^2, t is in min, and n_0 is the base line—i.e., initial value of carbon surface density.

The general form of the time-dependent portion of the right side of the equation can be written

$$n-n_0=\beta[1-\exp(-\alpha I_p)]t.$$

Here

$$\beta=\nu\epsilon,$$

where ν is molecules of hydrocarbons/cm^2 min and ϵ is the efficiency of conversion to carbon contaminant, and

$$\alpha=\sigma\tau,$$

where σ is the interaction cross section and τ is the residence time for hydrocarbon. Thus

$$n-n_0=\nu\epsilon[1-\exp(-\sigma\tau I_p)]t.$$

Let us consider the asymptotic forms of the equation. When $I_p\rightarrow\infty$,

$$n-n_0=\nu\epsilon t,$$

which is independent of proton current. This implies that the proton impingement saturates the surface with sites for conversion of hydrocarbons to carbon plus gases. Under these conditions the contamination depends solely upon the rate at which the hydrocarbons strike the surface, and, of course, the conversion efficiency.

When $I_p\rightarrow0$,

$$n-n_0=\nu\epsilon(\sigma\tau I_p)t=\epsilon(\nu\sigma\tau)I_pt$$

which indicates a linear dependence upon I_p. It may be interpreted then that under these conditions there is an apparent saturation with hydrocarbons and now the process depends upon the protons available for conversion. It has been observed that after 16 h with no beam on the target the contamination surface density remained constant. This carries the relation to the extreme $I_p=0$.

As further possible tests of the relation, experiments should be performed where ν is varied and where τ is varied. The tests required and the controls necessary fall deeply into the realm of surface science (chemistry and physics of surface phenomena) and are outside the scope of the present experiments.